Grid Generation for Wing-Tail-Fuselage Configurations

Arvin Shmilovich* and D. A. Caughey†
Cornell University, Ithaca, New York

An efficient procedure for generating boundary-conforming coordinate systems for three-dimensional wing-tail-body combinations is presented. A sequence of conformal and shearing transformations is employed to yield a slotted and nearly orthogonal computational domain and the resultant grid is nearly orthogonal almost everywhere. Computational grids for several realistic configurations are shown to illustrate the capability of the mesh generation procedure. The method is computationally more efficient than a number of other grid generation techniques, i.e., numerical methods or algebraic procedures; it allows for the control of orthogonality and requires less computational effort than one sweep of a transonic potential flow solver.

Nomenclature

a,b	= constants in azimuthal stretching functions; see Eqs. (2)
a_{ij}	= Fourier coefficients of fuselage cross section
A,B,C,D,E	= coefficients in stretching functions for wraparound coordinate
c	= section chord in constant $\bar{r}$ surface
d	= constant in azimuthal stretching functions; see Eqs. (2)
r	= radial coordinate in cross-flow plane
$\bar{r}$	= normalized radial coordinate; see Eq. (1)
R	= radius in cross plane
$S(\xi,\bar{r})$	= strip width after conformal mapping
x,y,z	= Cartesian coordinates; see Fig. 1
X,Y,Z	= computational coordinates; see Eq. (4)
θ	= azimuthal angle in cross-flow plane
$\bar{\theta}$	= normalized azimuthal angle; see Eq. (2)
ξ,η	= real and imaginary parts of complex variable in conformally mapped surfaces; see Eq. (3)

Subscripts

f	= fuselage
s	= singular line
t	= tip, tail
w	= wing

Introduction

IT is of practical interest to obtain solutions for the flow past realistic airplane configurations. The panel method has been proven useful in treating configurations of great geometrical complexity.[1] However, that method is applicable only to cases for which the flow is described by the linear potential equation. When treating transonic flows it is necessary to use finite difference (or finite element) field techniques that must be implemented within a suitable three-dimensional mesh system. In addition, if boundary conditions are to be enforced accurately, the mesh should be body-fitted. These demands have given added stimulus to the development of three-dimensional mesh generation techniques.

Received Aug. 12, 1984; revision received Feb. 21, 1985.

*Post-Doctoral Associate, Sibley School of Mechanical and Aerospace Engineering; currently, Senior Engineer/Scientist, Douglas Aircraft Company, Long Beach, California.

†Professor, Sibley School of Mechanical and Aerospace Engineering. Associate Fellow AIAA.

The topologies of boundary-conforming grids generally fall into three categories: O-, C-, and H-type grids. The topologies are suggested by these letters of the alphabet. O-type grids have one coordinate surface which wraps completely around the body; the conformal mapping of an airfoil to a circle is the most common example. C-type grids have one coordinate surface which wraps around the body and a branch cut extending to infinity (which is frequently used to represent a vortex sheet). H-type grids are nearly Cartesian, with the body included within a double-valued segment of one surface; a stream-function/potential-function coordinate system is an example of this grid type.

A useful numerical method for generating networks about rather arbitrary body shapes by solving systems of elliptic equations has been developed by Thompson et al.[2] However, this technique is generally computationally expensive (i.e., it frequently requires nearly the same computational expense as a transonic potential flow calculation).

Rubbert and Lee[3] have generated three-dimensional meshes for quite complex geometries by extending the standard Thompson approach. Their procedure produces an H-type mesh, unless a patching procedure is adopted, which in turn introduces irregularities in the immediate vicinity of the wing.

Jou and Mercer[4] have developed a mesh system for wing-tail-body combinations by embedding a C-type mesh for the tail into a global C-type mesh for the wing and fuselage. Their procedure does not result in a completely boundary-conforming system for the fuselage and the mesh is not orthogonal. Also, it is not well suited for treating a configuration whose tail is too close to the wing—the case in which the tail most affects the wing loading. Naturally, the flow calculation on such an overlapping system must be carried out on each of the subdomains independently, allowing for proper interaction at the interfacial boundary. Although the approach is quite straightforward, this last feature introduces considerable complexity into the coding. Moreover, since the location of the wake trailing behind the wing cannot be approximately aligned with a grid surface of the wraparound tail mesh, the jump condition for the velocity potential is enforced on the upper boundary of the tail domain. This effectively introduces a sharp discontinuity in the vertical displacement of the wing vortex sheet in the vicinity of the tail.

Two other related works should also be mentioned. The first is a mesh generation procedure similar to the authors' used by Jameson and Baker[5] for wing-tail-fuselage configurations. Baker and Jameson's procedure is based upon a parabolic mapping for the wing, which is then made to conform to the fuselage by suitable shearing transformations, with incorporation of the tail in a manner almost identical to

the present method. The second is the work of Eriksson and Rizzi,[6] who generated meshes for wing-canard combinations using a transfinite mapping procedure. Eriksson and Rizzi did not include the fuselage in their calculations. Both of these meshes were then used for computations using the Euler equations (rather than the potential equation, as in the present study).

Body-fitted coordinate systems are particularly attractive when generated by a transformation of the physical space into a simple computational domain such as a rectangular box. The procedure described herein uses this approach to generate grids for wing-tail-body configurations. The resulting mesh is of type C for the wing and type H for the tail. This procedure may be viewed as an extension of the wing-body grid generation sequence devised by Caughey and Jameson.[7] Throughout the paper these two classes of geometries will be referred to as the tail-on and tail-off configurations, respectively. The method of Caughey and Jameson is embodied in a computer code known as FLO-30, which analyzes the transonic potential flowfield for wing-body configurations. Use of FLO-30 is appropriate for predicting the transonic flow past simple wing-fuselage combinations, but it also can be used to estimate the aerodynamic loads upon configurations with tails, if the tail is sufficiently far downstream of the wing (as is usually the case for transport aircraft), so that its effect upon the wing pressure distribution is small. The correct treatment of the flow past tail-on configurations becomes more important when analyzing the flow past airplanes whose tails are very close to the trailing edge of the wing (as is frequently the case for fighter-type aircraft). In such instances the tailless model cannot be expected to produce a realistic flowfield and the inclusion of the tail is necessary to provide insight into the nature of the complete flow pattern.

The procedure presented here is computationally efficient. The generation of the mesh for the wing-tail-fuselage combination requires only about one and one-half times the amount of computational work of the mesh generation step for the tailless configuration, when both grids have the same number of nodes.

During the course of this work an attempt was also made to construct a grid having C-type meshes for both the wing and tail, but was not completely successful. Two candidate conformal mappings were derived following the systematic procedure suggested by Caughey,[8] but were abandoned because of the topological complexity of the meshes, especially for cases in which the tail plane is close to the plane of the wing. Further, the clustering of mesh lines in the vicinity of the lifting surfaces would have resulted in concentrations of mesh points in regions where they are not required for accuracy; a feature which, in a sense, defeats the purpose of generating a C-type mesh.

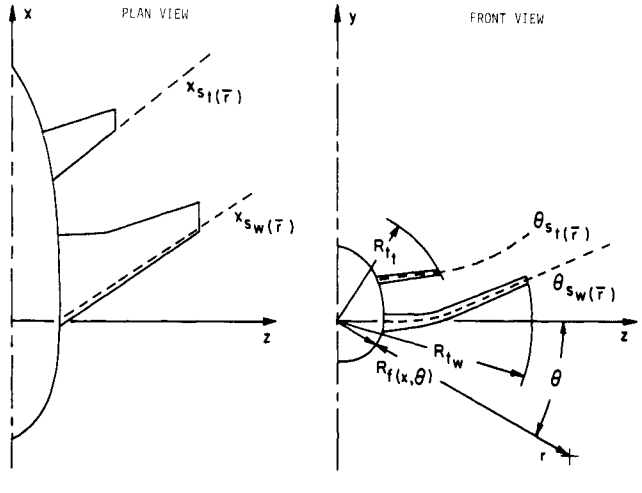

Fig. 1 Wing-tail-fuselage geometry.

A general outline of the mesh generation procedure will be presented in the next section, with the resulting grid geometries for several selected configurations presented in the section following that. Results of transonic potential flow calculations on these grids will be presented in a companion article. Further details of the grid generation procedure, flow computation, and additional examples are contained in Ref. 9.

Analysis

Wing-Horizontal Tail-Fuselage Arrangement

The cylindrical wind tunnel mapping described in Ref. 7 forms the point of departure for the mesh generation procedure of the wing-tail-fuselage combination. Consider the configuration shown in Fig. 1, which consists of a swept, tapered wing and tail of arbitrary planform, dihedral and section, mounted upon a fuselage of varying cross-sectional shape. The flow is assumed symmetrical about the vertical plane passing through the fuselage centerline so that only the flow in the half-space $z \geq 0$ need be considered.

Denoting the fuselage surface by $R_f(x,\theta)$, the radial coordinate is normalized by defining

$$\bar{r} = \frac{r - R_f(x,\theta)}{R_{t_w} - R_f(x,\theta)} \tag{1}$$

R_{t_w} being the radial coordinate of the wing tip. Normalized streamwise and azimuthal coordinates are also introduced as

$$\bar{x} = \frac{x - x_s(\bar{r})}{c(\bar{r})} + \log 2, \quad \bar{\theta} = b \mp \sqrt{d^2 - (\theta - a)^2} \tag{2}$$

where

$$a = \frac{2\theta_s^2 - \pi^2}{4\theta_s} = -b$$

$$d^2 = (\theta_s - a)^2 + a^2$$

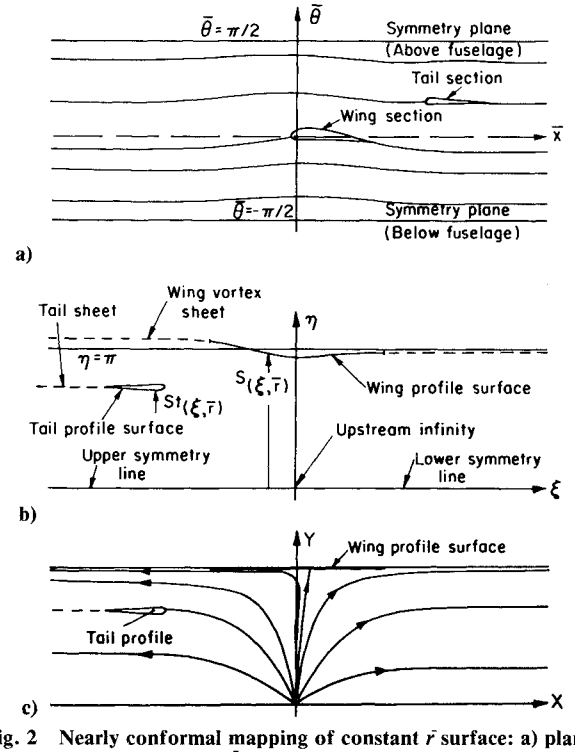

Fig. 2 Nearly conformal mapping of constant $\bar{r}$ surface: a) plane of normalized coordinates $\bar{x},\bar{\theta}$; b) conformally mapped plane; c) computational plane showing schematic streamlines.

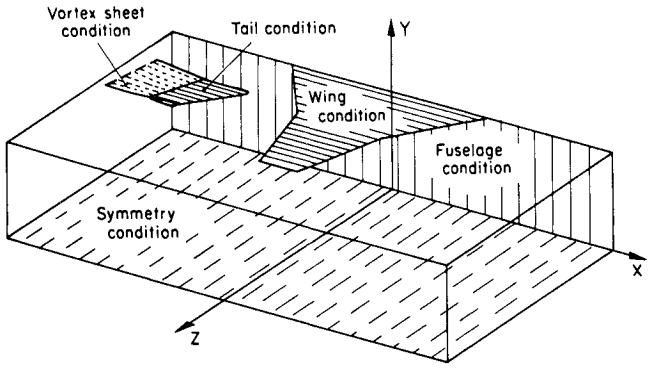

Fig. 3 Sketch of computational domain.

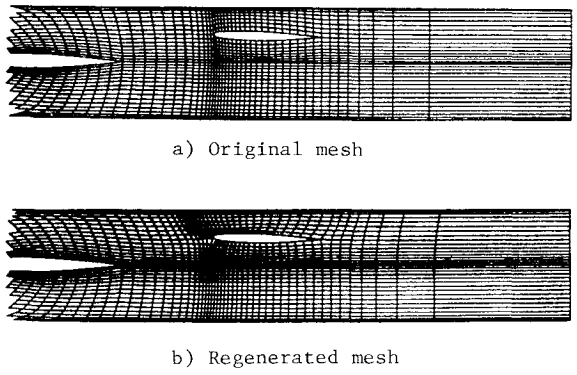

Fig. 4 Improvement of mesh orthogonality in the tail vicinity.

and the minus or plus sign is taken depending upon whether θ_s is positive or negative, $c(\bar{r})$ is the local chord, and $x_s(\bar{r})$ and $\theta_s(\bar{r})$ represent the coordinates of a singular line just inside the wing leading edge. The singular line is then used as a branch point in the conformal mapping

$$\bar{x}+2i\bar{\theta}=\log[1-\cosh(\xi+i\eta)] \tag{3}$$

to "unwrap" the wing surface. Under this transformation a surface of constant $\bar{r}$ which intersects both the wing and tail surfaces, shown in Fig. 2a, will take the form depicted in Fig. 2b. The contour of the tail section and its continuation downstream is described by a double-valued function $S_t(\xi,\bar{r})$. A final shearing transformation

$$X=\xi, \qquad Y=\eta/S(\xi,\bar{r}), \qquad Z=\bar{r} \tag{4}$$

maps the strip of width $S(\xi,\bar{r})$ to one of constant width, as shown in Fig. 2c.

The computational domain in Fig. 3 is rendered finite by suitable stretchings in the X and Z directions. These stretchings are chosen to ensure continuous first and second derivatives, and such that grid surfaces pass through the leading edges, trailing edges, and tips of both lifting surfaces, and also define a plane as the downstream boundary in the physical domain. An additional shearing in Y is employed to account for the finite thickness of the tail. These stretchings also control the concentration of grid points in regions where higher resolution is desired, such as near the leading edges of the lifting surfaces. The longitudinal stretching is set in each $\bar{r}$ surface, the angular stretching is set at every vertical line in the computational box, and the spanwise cell distribution is universal for all X and Y.

To account for lift, vortex sheets emanating from the trailing edges of the wing and the tail must be allowed (and are represented by the dashed lines in Fig. 2b). In the flow computation, the jumps in the velocity potential across the respective sheets are determined by the Kutta condition, and the mass flux balance resulting from a conservative formulation of the potential equation is satisfied at points that lie on them. The vortex surfaces are assumed to leave the trailing edges at their bisection angle smoothly, and the vortex sheet leaving the wing is taken as the branch cut of the conformal mapping.

The definition of $R_f(x,\theta)$, $S(\xi,\bar{r})$, and $S_t(\xi,\bar{r})$ from the input data of the fuselage, wing, and tail geometry, and the associated vortex surfaces, is achieved by spline fits. At each station, the Fourier decomposition of R_f

$$R_f(x_i,\theta)=\sum_{j=1}^{m} a_{ij}\cos j(\theta+\pi/2) \tag{5}$$

is used to determine the coefficients a_{ij}. Since the fuselage is assumed symmetrical about the plane $\theta=\pm\pi/2$, only the cosine terms need be considered, provided that the point about which the decomposition is made lies on the plane of symmetry. The origin may be chosen to lie anywhere within the section, the only requirement being that the Fourier representation remain single-valued. Most commonly it is chosen as the centroid of the cross section.

The wing and tail cross sections are input at a number of spanwise stations. A spline fit in x is used to interpolate the coefficients of the fuselage cross section in mapping wing and tail geometries to the $\bar{x},\bar{\theta},\bar{r}$ system. A spline fit in the $\bar{r}$ direction is employed to obtain the images of the wing and the tail sections and the associated vortex sheets in each computational surface $\bar{r}=$ const. If the lifting surface is not oriented approximately in the radial direction, more spanwise input sections are needed in order that the $\bar{r}$-wise interpolation will not introduce inaccuracies in its geometrical definition. One such extreme case is a low-lifting surface having dihedral. The conformal mapping of Eq. (3) is applied in each $\bar{r}$ surface and the determination of the mesh points in each surface is accomplished by spline fitting upon $S(\xi,\bar{r})$ and $S_t(\xi,\bar{r})$ in the ξ direction. Having defined a_{ij}, S, and S_t, we can proceed to calculate the physical coordinates of the grid points by reversing the mapping sequence.

This mapping sequence results in a C-type mesh for the wing and an H-type mesh for the tail. The procedure is not suitable for treating vertical tails lying in the plane of symmetry.

The procedure for treating a low tail follows the same steps as for a high tail, but the definition of the curve S_t is different. The image of a tail located below the wing plane will appear in the half-box $X>0$ of Fig. 3. An earlier version of the mesh generator was specialized to construct meshes about either low or high tails. However, generalization of the flow algorithm to treat both cases was abandoned since it would have resulted in a cumbersome code. The present code is suitable for high tail combinations, but a slight modification of the way the input data is supplied to the program will allow it to treat low tails: Since the mirror image of the low tail configuration about the x-z plane is a high tail arrangement, an auxiliary routine which reflects the input coordinates of the fuselage and the lifting surfaces about the horizontal plane can be used to provide the program with proper input. Also, the signs of angles defined in the x-y and y-z planes need be reversed (the angle of attack, tail deflection, and dihedral angles).

The question naturally arises whether the tail-on mesh generation procedure is more expensive than that used for the tailless configuration. Obviously, more mesh lines are needed for the tail-on configuration to meet the requirement of reasonable resolution in the vicinity of the tail. Nevertheless, ignoring a negligible additional overhead, the computational work required per mesh point for the tail-on configuration is only about 50% more than the tailless combination. The additional overhead arises from the need to handle the additional input data required to define the tail surface, which has to be interpolated upon, and because of the more complicated stretching functions required.

A local refinement of the H-type grid in the vicinity of the tail to a more nearly orthogonal mesh may be desirable. To accomplish this, a portion of the mesh in each X, Y plane surrounding the tail is regenerated using a sequence of conformal transformations to map the tail section onto a slit. Referring to Fig. 2, an obvious choice for the refined domain is that part of the grid bounded by an X mesh line upstream of the tail and extending downstream to the far-field boundary, between the upper symmetry line and the branch cut. The distance of the tail from the wing is unimportant since the refined domain can also be partly bounded by the upper surface of the wing. More specifically, a Joukowsky transformation is first used to map the tail section onto a noncentered, nearly circular contour. Next, a displacement transformation is utilized to center the near circle, followed by application of the complex potential for a rotating circular cylinder in freestream to map the nearly circular contour onto a near slit while maintaining orthogonality near the horizontal boundaries. A smooth transition between the global and refined grids can be guaranteed by a smooth construction of the grid in the local (nearly rectangular) transformed plane, since the mesh points on the interfacial boundaries are the same. Reversal of the mapping sequence will yield a more orthogonal mesh near the tail as shown in Fig. 4.

Wing-Double Twin Tail-Fuselage Arrangement

It is also feasible to generate a grid for the configuration that has an empennage consisting of twin vertical fins as well as twin horizontal tails, such as shown in Fig. 5. The procedure for this case can be synthesized from the above procedure, utilizing additional stretchings within the domain.

First, the $\bar{r}$ cylindrical surfaces are distributed such that the innermost plane defines the fuselage and three other planes pass through the tips of the tails and wing.

The construction of the mesh about wing-double twin tail-body combinations is facilitated by the fact that the vortex sheet trailing behind the wing passes between the tails. This holds for most such airplanes. The vertical fin may be regarded as a high tail, and the horizontal fin as a low tail. Application of the conformal map Eq. (3) to an $\bar{r}$ surface which intersects all lifting surfaces yields the computational plane depicted in Fig. 6a. The vertical tail is mapped to the half-plane $X<0$, while the image of the horizontal tail lies in the other half.

The same number of cells in the angular direction, between the branch cut and each of the tails, is chosen. Consequently, in each X, Y plane a dividing Y line is partly described by a function S_t, which passes through both tail sections and their associated vortex sheets. The definition of the curve S_t has to be extended to include the gap between the leading edges of the tails. The midpart of the curve is defined by a horizontal line whose endpoints 1 and 2 are at the same distance from the Y axis. These points are connected to the corresponding leading edges of the tails by slowly varying curves. The Y level of the midcurve opposite the leading edge of the wing controls the amount of bunching of the grid lines near the wing. It was found necessary to incorporate this constraint in the definition of S_t to produce proper C grid lines about the wing.

If the horizontal and vertical tails are at approximately the same axial location, the additional resolution of a relatively dense H-type mesh efficiently resolves the solution in the vicinity of both surfaces. The same number of cells in the longitudinal direction was put on each tail planform. Also, the same number of cells was put between the wing and each of the tails.

To simplify the treatment of the mass flux balance on the vortex sheet emanating from the wing, the distribution of the mesh points on the cut must be symmetric about $X=0$. Therefore, the leading and trailing edges of the tails are connected by mesh lines which cross the cut smoothly in each X, Y plane. These lines satisfy $-X_{e'}=X_e$ and $-X_{b'}=X_b$ at $Y=1$; represented by the solid vertical lines in Fig. 6a. The locations of points b and e are chosen as suitable averages of the X coordinates of the leading edges (X_a and X_c) and the trailing edges (X_d and X_f), respectively.

On $Y=1$ the cells are distributed according to a prescribed X stretching. This will be called a nominal distribution since on any other Y grid line, a shearing in X must be employed and the distribution is no longer symmetrical about $X=0$. The horizontal shifts of the leading and trailing edges of the tails are calculated from the nominal distribution. As an example, for the low tail the differences $\Delta X_{ab}=X_b-X_a$ and $\Delta X_{ed}=X_e-X_d$ are taken. Next, on each half-plane the cells are distributed on S_t according to curves of the form

$$\Delta X=A+BX+C\sin(DX)+E\sin(2DX) \qquad (6)$$

for the perturbation of the X coordinate from the nominal stretching. Thus, the X distribution on S_t is formed by superposition of ΔX on the nominal one. Here $\Delta X=(\Delta X)'=(\Delta X)''=0$ at $X=0$ and $X=X_4$ are chosen so that the

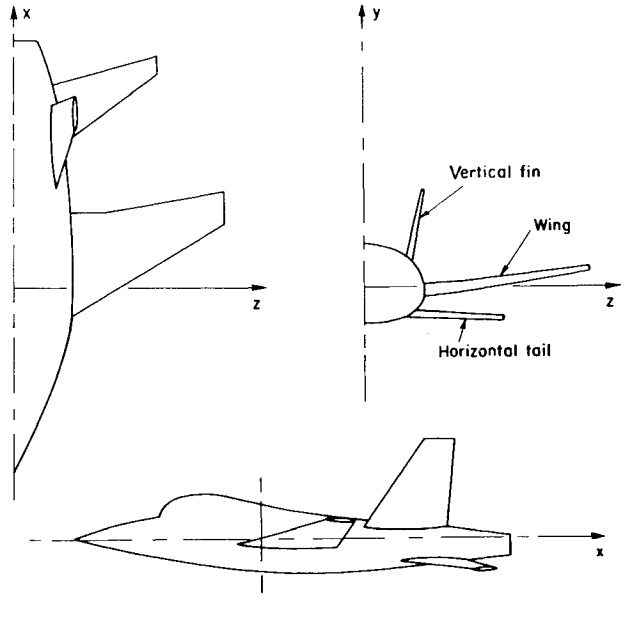

Fig. 5 Geometry of airplane with double twin tail empennage.

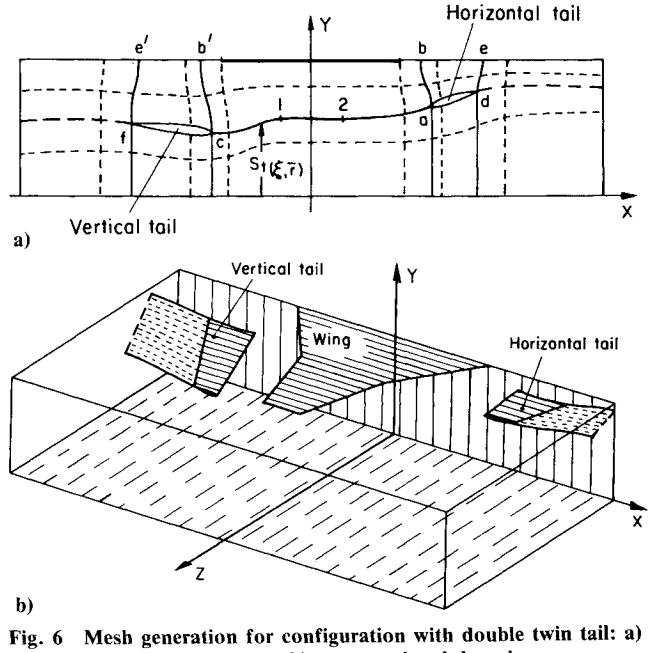

Fig. 6 Mesh generation for configuration with double twin tail: a) layout of mesh in X, y plane; b) computational domain.

mesh will undergo minimal distortion ahead of the leading edge of the wing, and the downstream boundary will still be a plane. Moreover, the constraints on $(\Delta X)_{X=0}$ ensure smooth second derivatives across $X=0$ where the stretchings are matched from either side.

The X-wise distribution used on S_t is used along all of the Y lines below S_t also. Above the horizontal division line ΔX is varied along each X mesh line, ensuring perpendicularity at the branch cut.

Incorporation of the angular stretching along each X line completes the construction of the network. Some of the resulting grid lines are represented in Fig. 6a by dashed lines. The resulting computational box is shown in Fig. 6b. In this figure, the associated vortex sheets are represented by the fine dashed surfaces.

For a conventional (nearly horizontal) lifting surface several cuts are made to define the input section data at a number of spanwise stations, whereas for the proper description of the sections of a vertical fin, horizontal cuts are needed at several vertical stations. In addition, a vortex surface is shed downstream of the vertical tail and its horizontal displacement is defined in a manner similar to that of the vertical displacement of the vortex sheets corresponding to the horizontal lifting surfaces.

It should be noted that there are instances for which modifications of the prescribed procedure might be desirable. If, for example, a different number of cells is desired between the branch cut and each of the tails, the definition of S_t will no longer be adequate. Two such curves would have to be defined, each one partly consisting of one of the tails and its associated sheet. Consequently, a more complicated angular stretching function would be required.

Results

Several existing aircraft were used to exercise the capability of the mesh generation program in treating tails of arbitrary planform. The variety of planforms of the lifting surfaces and their location relative to each other was helpful in refining and generalizing the mesh generation sequence. Since, for most of the examples to be presented, accurate geometrical data were not available, the configurational data were gleaned from the semipopular literature.

Figure 7 displays cuts through the network generated for the ONERA wing M-6 and a tail whose cross section is identical to the wing section, mounted upon a cylindrical body.

A more difficult case is presented by an aircraft whose tail continuation in the spanwise direction crosses the vortex sheet of the wing (or its continuation). Referring to Fig. 1b, imagine the tail or wing as relocated and reoriented so that the two dashed lines coalesce at one span station. As a consequence, study of Fig. 2 reveals that on those cylindrical $\bar{r}$ surfaces close to the fuselage, the tail section will lie in the half-strip $\xi<0$, while on those $\bar{r}$ surfaces far from the fuselage, its continuation will lie in the other half. Resolution of this difficulty is achieved by specifying a suitable spanwise location for the extension outboard of the tip of the mesh line passing through the leading edge of the tail. The McDonnell F-4, which has a tail higher than the wing but with a large tail anhedral angle, was chosen to be the representative of such cases. Views of this mesh are presented in Fig. 8. Similar problems might arise for cases in which the fuselage is very thin at the root section of the tail, or for cases in which the tail is at high incidence.

The final example is a mesh generated for a wing and a tail unit that consists of twin vertical fins and twin horizontal tails that protrude from the fuselage. A separate program was coded to treat such combinations. The grid was generated for

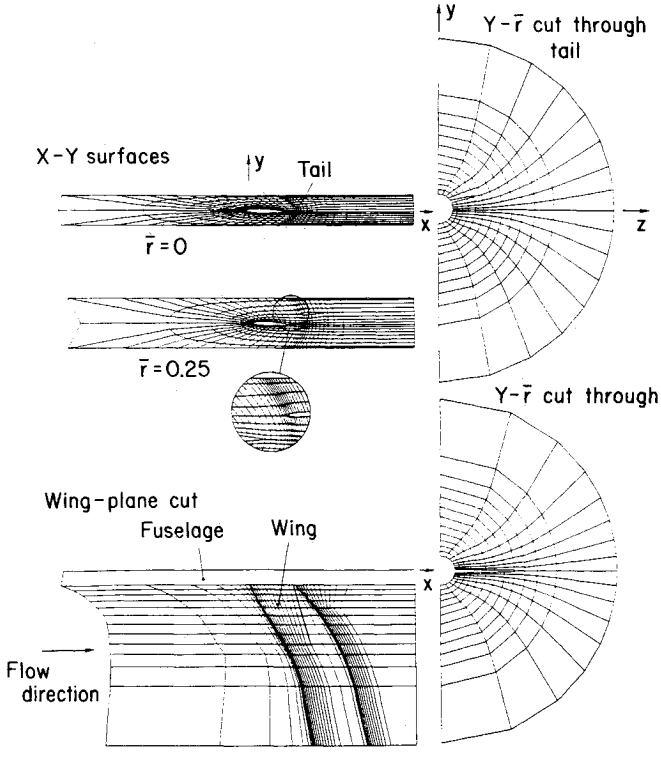

Fig. 7 Silhouettes of grid for the ONERA arrangement.

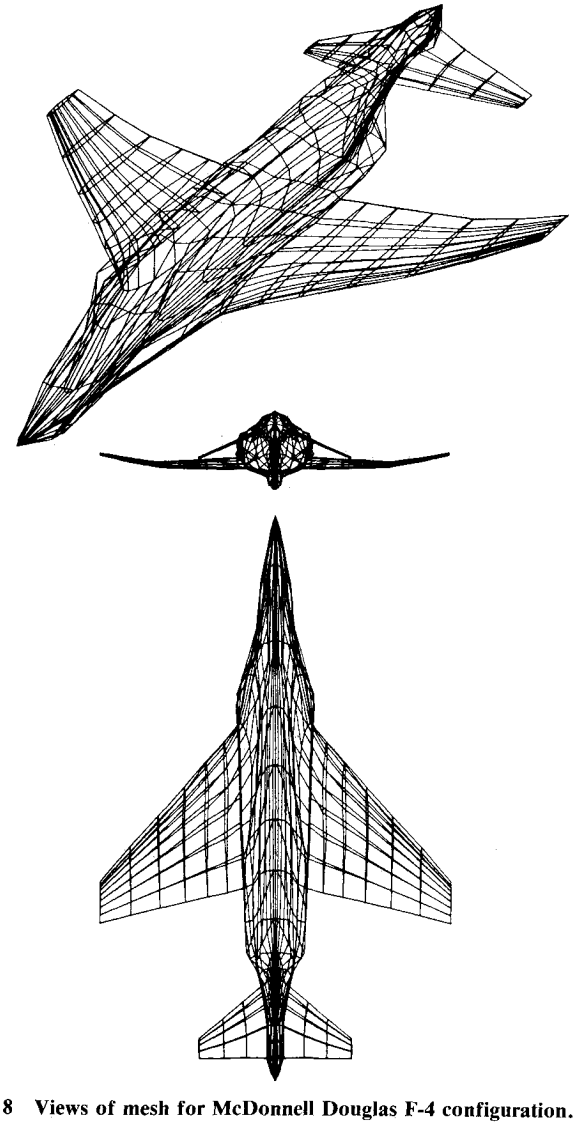

Fig. 8 Views of mesh for McDonnell Douglas F-4 configuration.

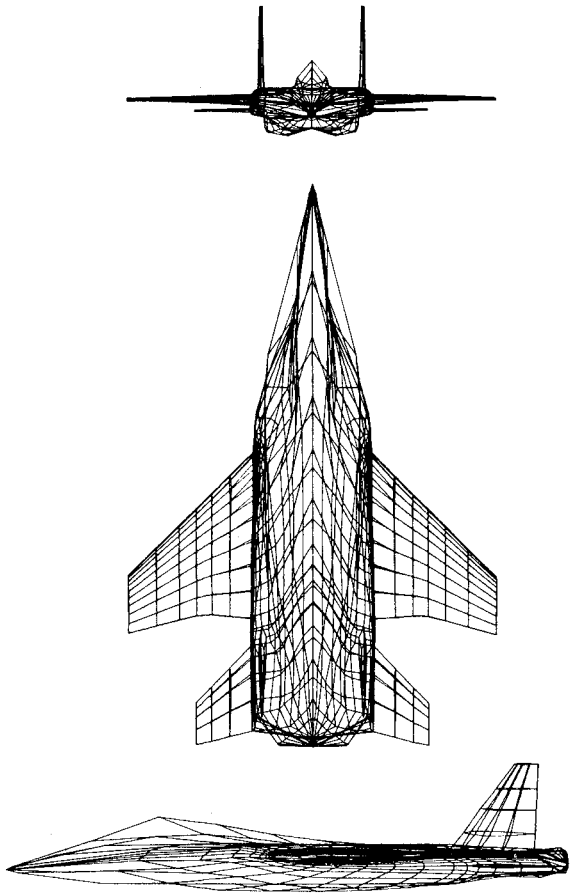

Fig. 9 Views of mesh for McDonnell Douglas F-15 configuration.

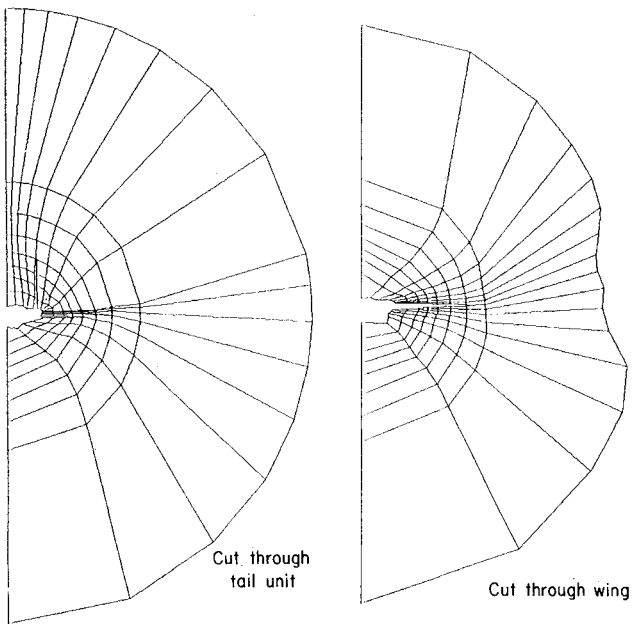

Fig. 10 *Y-Z* cuts through empennage and wing of mesh generated for the combination in Fig. 9.

the McDonnell Douglas F-15 aircraft, and is shown in Fig. 9. Representative cuts of the associated grid network are plotted in Fig. 10.

The grids described herein are presently being used in the development of transonic potential flow analysis methods. These methods are based upon a multigrid implementation (Refs. 10 and 11) of the finite volume algorithm described in Refs. 12 and 13, and will be reported upon in a companion article.[14]

Conclusion

An efficient procedure has been developed for generating boundary-conforming coordinate systems for three-dimensional wing-tail-body combinations. The meshes were originally developed for transonic potential flow calculations, but should also be useful for computations using finite volume formulations of the Euler equations. The method is based upon a sequence of conformal and shearing transformations, and is capable of treating a wide variety of aircraft including high- and low-tail configurations as well as some twin-tail geometries. The procedure produces a grid having a C-type topology for the wing and an H-type topology for the tail surfaces. The method is very efficient computationally, requiring less computer time than one sweep of a transonic potential flow solver on the grid generated.

Acknowledgment

This work has been supported in part by the Office of Naval Research under Contract N00014-77-C-0033.

References

[1]Krause, W., "Panel Methods in Aerodynamics," *Numerical Methods in Fluid Dynamics*, edited by H. J. Wirz and J. J. Smolderen, Hemisphere Publishing Corp., Washington, D.C., 1978, pp. 237-298.

[2]Thompson, J. F., Thames, F. C., and Mastin, C. M., "Automatic Numerical Generation of Body-Fitted Curvilinear Coordinate System for Field Containing any Number of Arbitrary Two-Dimensional Bodies," *Journal of Computational Physics*, Vol. 15, 1974, pp. 299-319.

[3]Rubbert, P. E. and Lee, K. D., "Patched Coordinate Systems," *Numerical Grid Generation*, edited by J. F. Thompson, North-Holland Publishing Co., New York, 1982, pp. 235-252.

[4]Jou, W. H. and Mercer, J. E., "Mesh Generation for Wing-Body-Tail Combinations," *Advances in Grid Generation*, edited by K. N. Ghia and U. Ghia, American Society of Mechanical Engineers, New York, 1983, pp. 167-172.

[5]Jameson, A. and Baker, T. J., "Multigrid Solution of the Euler Equations for Aircraft Configurations," AIAA Paper 84-0093, Jan. 1984.

[6]Eriksson, L.-E. and Rizzi, A., "Computation of Vortex Flow around a Canard/Delta Combination," *Journal of Aircraft*, Vol. 11, Nov. 1984, pp. 858-865.

[7]Caughey, D. A. and Jameson, A., "Numerical Calculation of Transonic Potential Flow about Wing-Body Combinations," *AIAA Journal*, Vol. 17, Feb. 1979, pp. 175-181.

[8]Caughey, D. A., "A Systematic Procedure for Generating Useful Conformal Mappings," *International Journal for Numerical Methods in Engineering*, Vol. 12, Nov. 1978, pp. 1651-1657.

[9]Shmilovich, A., "Calculation of Transonic Potential Flow past Wing-Tail-Fuselage Configurations Using the Multigrid Method," Ph.D. Thesis, Cornell University, Ithaca, N. Y., 1984.

[10]Shmilovich, A. and Caughey, D. A., "Application of the Multigrid Method to Calculations of Transonic Potential Flow about Wing-Fuselage Combinations," *Journal of Computational Physics*, Dec. 1982, pp. 462-484.

[11]Caughey, D. A., "Multi-Grid Calculation of Three-Dimensional Transonic Potential Flows," *Applied Mathematics and Computation*, Vol. 13, 1983, pp. 241-260.

[12]Jameson, A. and Caughey, D. A., "A Finite-Volume Method for Transonic Potential Flow Calculations," *Proceedings of the AIAA 3rd Computational Fluid Dynamics Conference*, Albuquerque, N. Mex., June 1977, pp. 35-54.

[13]Caughey, D. A. and Jameson, A., "Progress in Finite-Volume Calculations for Wing-Fuselage Combinations," *AIAA Journal*, Vol. 18, Nov. 1980, pp. 1281-1288.

[14]Shmilovich, A. and Caughey, D. A., "Multigrid Calculation of Transonic Flow past Wing-Tail-Fuselage Combinations," (to be published, *Journal of Aircraft*).